Key Engineering Materials
ISSN: 1662-9795, Vol. 926, pp 2211-2221
doi:10.4028/p-33un7m

Submitted: 2021-12-11
Revised: 2022-01-20
Accepted: 2022-01-21
Online: 2022-07-22

Identification of Swift Law Parameters Using FEMU by a Synthetic Image DIC-Based Approach

João Henriques[1,a*], Mariana Conde[1,b], António Andrade-Campos[1,c], and José Xavier[2,d]

[1]TEMA, Department of Mechanical Engineering, University of Aveiro, Campus Universitário de Santiago, 3810-193 Aveiro, Portugal

[2]UNIDEMI, Department of Mechanical and Industrial Engineering, NOVA School of Science and Technology, NOVA University Lisbon, 2829-516 Caparica, Portugal

[a]joaodiogofh@ua.pt, [b]marianaconde@ua.pt, [c]gilac@ua.pt, [d]jmc.xavier@fct.unl.pt

Keywords: Inverse Identification, Digital Image Correlation, Synthetic Image, Finite Element Model Updating, Finite Element Analysis

Abstract. Computer-aided engineering systems rely on constitutive models and their parameters to describe the material behaviour. The calibration of more elaborated material models with a larger number of parameters becomes very time and cost consuming. The development of image-based technology has enhanced the interest in inverse identification methods, which, when coupled with full-field measurements, have the potential to reduce the number of experimental tests required to accurately identify material properties. This work aims to identify the Swift hardening law parameters of a dual-phase steel using a tensile test on a heterogeneous dogbone specimen under uniaxial and quasi-static loading conditions using the finite element model updating (FEMU) technique. The numerical results were used to generate synthetic images, which were then processed by digital image correlation (DIC) and used as the reference in the identification procedure. Two different approaches were tested: (i) directly comparing the numerical results to the reference; (ii) using DIC-levelled numerical data by iteratively generating synthetic images and using the DIC filter with the same settings as were used on the reference (virtual experiment). The identification results obtained from both approaches are compared and discussed.

Introduction

Computer-aided engineering systems play a key role in the simulation of manufacturing processes, in order to reduce costs and time-waste in the development of high-quality products. The material constitutive model and its parameters influence the reliability and accuracy of metal forming simulations. Although finite element analysis (FEA) is widely used to simulate processes, the accuracy of the simulation highly depends on the calibration of the model that describes the material behaviour.

In the recent decades, the scientific community has made significant efforts to develop precise constitutive model formulations in elastoplasticity [1, 2], including complex yield functions, isotropic and kinematic hardening models [2], and other advanced formulations [3]. However, the calibration of material constitutive models is still facing open challenges [4]. Furthermore, for more elaborated material models with a larger number of parameters, the calibration process becomes more complex and time-consuming [5].

Classical approaches involve identifying the material parameters through a series of classical mechanical tests that produce a quasi-homogeneous strain field at the gauge section [6]. The material parameters are then identified with post-treatment based on analytical expressions for the stress and strain components. Nevertheless, due to the simplified geometry and loading conditions, only a limited number of parameters can be identified per test configuration. However, as the number of experimental tests and material parameters increases, the experimental identification becomes increasingly difficult [7]. In order to solve this issue, inverse identification strategies must be used.

Given the recent advancements in image-based technology, there has been an increase in the use of novel optical methodologies in solid and fluid experimental mechanics, which are contact-free and provide full-field data. Among these techniques, digital image correlation (DIC) [8, 9, 10] has grown in popularity in recent years due to its relative ease of use, while also providing a good balance between spatial resolution and accuracy. This technological advancement was followed by the development of inverse identification methods to calibrate complex material models [11], most notably the finite element method updating (FEMU) method [12, 13, 14] and the virtual fields method (VFM) [15]. This approach has the potential to reduce the number of experimental tests required to accurately identify all material properties, given that the test configuration is rich enough so that all material properties play a role in the mechanical behaviour.

Experimental validation of FEA is crucial for developing confidence in numerical model predictions. Traditionally, experimental DIC measurements and FEA results were compared directly in the FEMU approach. However, numerous inconsistencies must be addressed before doing this comparison, including different coordinate systems, data locations, strain formulation, spatial resolutions, and data filtering. To address these issues, recent studies used an approach based on deforming the reference image of a DIC speckle pattern synthetically, using the FEA mesh and displacements [16, 17, 18]. The synthetically deformed images can then be processed with DIC using the same DIC settings as the experimental results, ensuring that both sets of data have the same filtering, spatial resolution, and strain formulation, while also avoiding additional interpolation steps. In addition, some pattern-related image artefacts, such as saturation, aliasing and lightning issues, may be easier to distinguish from actual model problems [17].

The goal of this work is to identify the Swift hardening law parameters of the DP600 steel by simulating a tensile test on a heterogeneous dogbone specimen with non-constant section [19] under uniaxial and quasi-static loading conditions up to rupture. The numerical results were used to generate synthetic images that were then processed by DIC and used as a reference in the identification procedure. The material parameters were identified using a FEMU approach, with a cost function that describes the difference between the reference and iterative numerical results, including the strain fields and load. Two approaches were tested: (i) directly comparing the reference with the FEA results, referred to as the FEA methodology and (ii) using DIC-levelled FEA data in the comparison with the reference, by iteratively generating synthetically deformed images and further processing them with DIC with the same settings used on the reference, referred to as the virtual experiment (VE) methodology.

Methodology

Tensile Test and Numerical Model. In this work, a virtual test was carried out on a heterogeneous dogbone specimen with non-constant section [19] under uniaxial tensile loading conditions. The specimen geometry and boundary conditions of the tensile test are shown in Fig. 1. This specimen geometry offers a heterogeneous strain field across a wide region, although the gradient of deformation is mostly along the y-direction [19].

A finite element analysis (FEA) model was implemented in ABAQUS/Standard software [20] assuming plane stress conditions. Moreover, the four-node plane stress element (CPS4R) is used and the mesh is defined as regular, with a total of 858 elements. A user-defined material subroutine, Unified Material Model Driver for Plasticity (UMMDp) [21], is used to model the material behaviour. The boundary conditions were imposed as displacements along the y-direction on the top boundary of the specimen and fixed as 0 on the bottom boundary. The test was conducted until the failure of the specimen, with a total of 10 time stages.

Material and Constitutive Model. The material used in this study is the DP600 steel, and the constitutive model chosen assumes the following considerations: (i) isotropic linear elastic behaviour according to Hooke's Law, (ii) isotropic hardening described by Swift law $\sigma = K(\varepsilon_0 + \bar{\varepsilon}^{\mathrm{P}})^n$ and (iii)

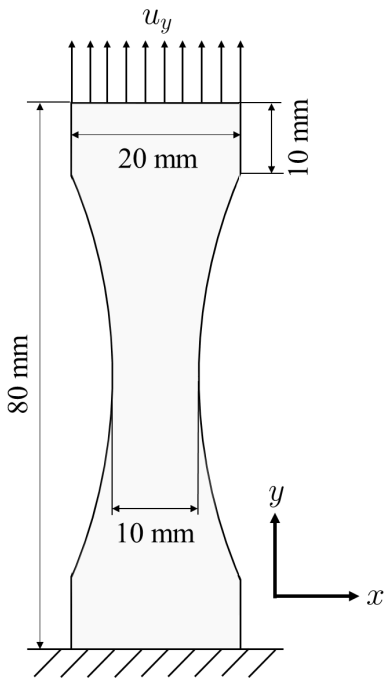

Fig. 1: Tensile test setup regarding the specimen geometry and boundary conditions.

anisotropic behaviour described by Yld2000-2d criterion for plane stress conditions. The goal of this work is to identify the material constitutive parameters related to the hardening behaviour. Therefore, the linear elastic parameters are fixed during the identification procedure. The modulus of elasticity (E) and the *Poisson*'s ratio (ν) are assumed to be 210 GPa and 0.3, respectively. The constitutive parameters of the Yld2000-2d criterion are also known during the iterative process and assumed as the reference values [22, 23]: $\alpha_1 = 1.011$, $\alpha_2 = 0.964$, $\alpha_3 = 1.191$, $\alpha_4 = 0.995$, $\alpha_5 = 1.011$, $\alpha_6 = 1.018$, $\alpha_7 = 0.977$, $\alpha_8 = 0.935$, $\alpha = 6$. The Forming Limit Diagram (FLD) was used as the rupture criteria, and the Swift law material parameters were calibrated, totaling three parameters to be identified. The reference Swift law parameters for the DP600 steel [22, 23] are presented in Table 2.

Synthetic Images. The reference numerical results, including the mesh and displacement fields, were used to generate synthetic images based on a real speckle pattern image using the MatchID FE Deformation module [24], which were then processed by DIC. The goal of this approach is to simulate a real experiment in which the experimental results are obtained using the DIC filter.

In the FEMU method, the main goal is to match the iterative numerical results to the experimental data, which is usually processed by DIC. However, several inconsistencies must be addressed, such as different coordinate systems, data locations, strain formulations, spatial resolutions, and data filtering. To address these issues, the iterative numerical results are used to synthetically deform the reference image of a real DIC speckle pattern, resulting in a set of synthetically deformed images. Afterwards, the synthetically deformed images can be processed with DIC using the same DIC parameters as the experimental images, ensuring that data filtering, spatial resolution, and strain formulation are consistent across both data sets. Furthermore, since this approach uses a real image of a speckle pattern, the experimental error sources are also included in DIC-levelled FEA data. As a consequence, pattern-related image artefacts like aliasing, lightning issues, and saturation can be easily distinguished from model flaws [17]. Fig. 2 shows a diagram of the VE methodology, including the comparison between the reference and VE results.

Digital Image Correlation. Using the MatchID software [24], the subset-based 2D-DIC technique was used to measure the displacements and strain fields across the entire region of interest (ROI) of the specimen. The selection of the DIC parameters set is critical and influences the results. This selection was performed using MatchID Performance Analysis module [24], with different sets of parameters

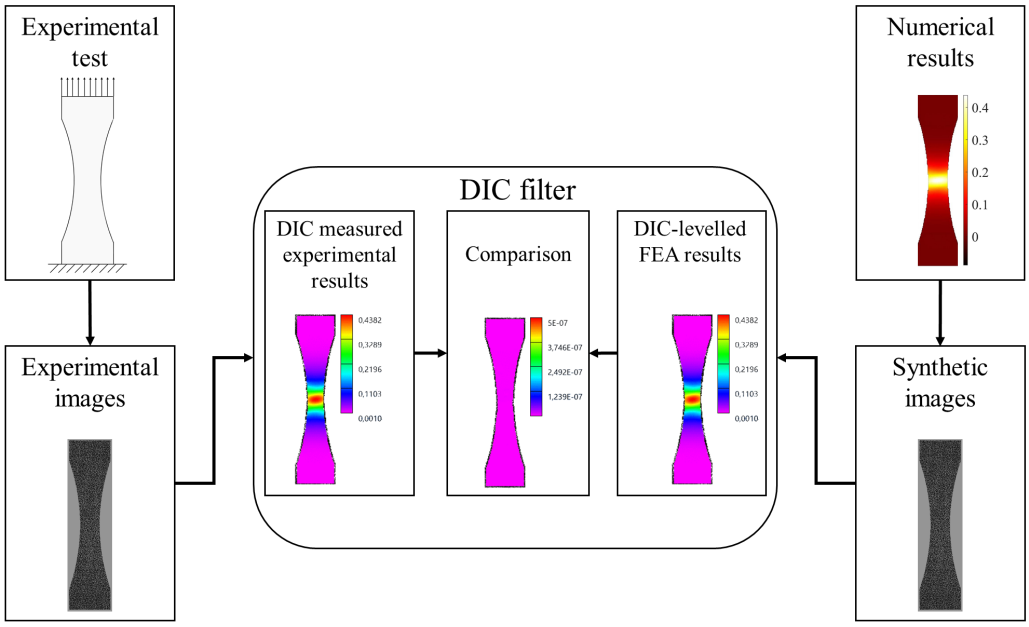

Fig. 2: Diagram of the VE methodology.

combinations for two selected stages (stage 7 and 10). A total of 192 analyses were carried out, using Affine/Quadratic subset shape functions, bilinear Q4/biquadratic Q8 strain interpolation, subset sizes ranging from 9 to 57 pixels (6 pixels increment), a fixed step size of 5 pixels and strain window sizes ranging between 5 and 35 data points (6 data points increments) which relates to a virtual strain gauge (VSG) size varying from 35 to 227 pixels.
The signal measured for the strain component on the y direction was compared to the VSG size for a central point on the specimen, where the most strain gradients are expected. It should be noted that the reference image used to generate the synthetic images was captured with a real camera in the experimental conditions and, therefore, the noise from the experimental setup, such as lightning issues and camera noise, is also included in the synthetic images. With this in mind, a balance between accuracy and spatial resolution must be found. Therefore, the selected set of settings is within a convergence band of DIC settings, where an increase in VSG and loss of spatial resolution have no noticeable effect on the measured signal. The 2D-DIC parameters used in this study are listed in Table 1.

Finite Element Model Updating Technique. The material constitutive parameters are identified using the FEMU approach. In this technique, an optimisation procedure is used to iteratively update the unknown material parameters set in order to minimize a cost function that reflects the differences between the reference DIC measurements and FEA results. In this work, two different approaches are investigated: (i) directly comparing the FEA results to the reference measurements (FEA methodology) and (ii) iteratively generating DIC-levelled FEA results and comparing them to the reference (VE methodology, as represented in Fig. 2). The MatchID FE Validation module [24] is used in the DIC-levelled FEA approach to process the iteratively generated synthetic images with DIC, using the same setting parameters and ROI as in the reference analysis. Fig. 3 shows a flowchart describing the parameter identification process using FEMU for the FEA and VE methodologies. The flowchart is separated into three main parts: (i) the generation of the reference virtual experimental strain fields and load data (see Fig. 3.a), (ii) the iterative process while using the FEA methodology (see Fig. 3.b) and (iii) the iterative process with the VE methodology (see Fig. 3.c).
The cost function used in this work describes the difference in strain fields and load between the reference and the iterative numerical results and is written as:

Table 1: 2D-DIC settings used for the full-field measurements, using MatchID software [24].

2D-DIC setting parameters	
Camera	Flir Blackfly BFS-U3-51S5M-C
Focal length	12.5 mm
Image resolution	2448×2048 px^2
Camera noise	0.48% of range
Working distance	251 mm
Image conversion factor	0.05039 mm/px
Speckle pattern	Numerically generated
Average speckle size	3 px
Correlation criterion	ZNSSD
Interpolation	Bicubic spline
Subset shape function	Quadratic
Subset size	21 px
Step size	5 px
Image pre-filtering	Gaussian, 5 px kernel
Strain window size	11
Strain interpolation	Bilinear Q4
Strain convention	Green-Lagrange
Displacement noise-floor	0.009 px, 0.446 µm
Strain noise-floor	1.246×10^{-4}

$$f(\boldsymbol{\chi}) = \frac{1}{n_\mathrm{t}} \sum_{i=1}^{n_\mathrm{t}} \left\{ \frac{1}{3n_\mathrm{p}} \sum_{j=1}^{n_\mathrm{p}} \left[\left(\frac{\varepsilon_{xx}^{\mathrm{num}}(\boldsymbol{\chi}) - \varepsilon_{xx}^{\mathrm{exp}}}{\varepsilon_{\mathrm{max}}^{\mathrm{exp}}} \right)^2 + \left(\frac{\varepsilon_{yy}^{\mathrm{num}}(\boldsymbol{\chi}) - \varepsilon_{yy}^{\mathrm{exp}}}{\varepsilon_{\mathrm{max}}^{\mathrm{exp}}} \right)^2 + \left(\frac{\varepsilon_{xy}^{\mathrm{num}}(\boldsymbol{\chi}) - \varepsilon_{xy}^{\mathrm{exp}}}{\varepsilon_{\mathrm{max}}^{\mathrm{exp}}} \right)^2 \right]_j + \left(\frac{F^{\mathrm{num}}(\boldsymbol{\chi}) - F^{\mathrm{exp}}}{F_{\mathrm{max}}^{\mathrm{exp}}} \right)^2 \right\}_i, \tag{1}$$

where $\boldsymbol{\chi}$ is the unknown material parameters set, n_t and n_p are the total number of time steps and full-field measurement data points, respectively. ε_{xx}, ε_{yy} and ε_{xy} are the different components of in-plane strain fields and F is the load. The superscripts "num" and "exp" represent the numerical and reference virtual experimental data, respectively, while the subscript "max" refers to the maximum value of the given component.

Using the ScyPy Python library [25], the Levenberg–Marquardt method, which is a gradient-based algorithm, was implemented.

Results and Discussion

The differences between the reference and iterative strain measurements and load results are minimised, with the optimisation variables being the constitutive parameters of the Swift law. Two identification runs with differing initial sets of parameters were performed for both methodologies described in this study. Table 2 lists the reference Swift law parameters for the DP600 steel [22, 23], the lower and upper bounds for each parameter during the identification process, the initial set of parameters used for each identification run, the cost function value, the identification results, including the rel-

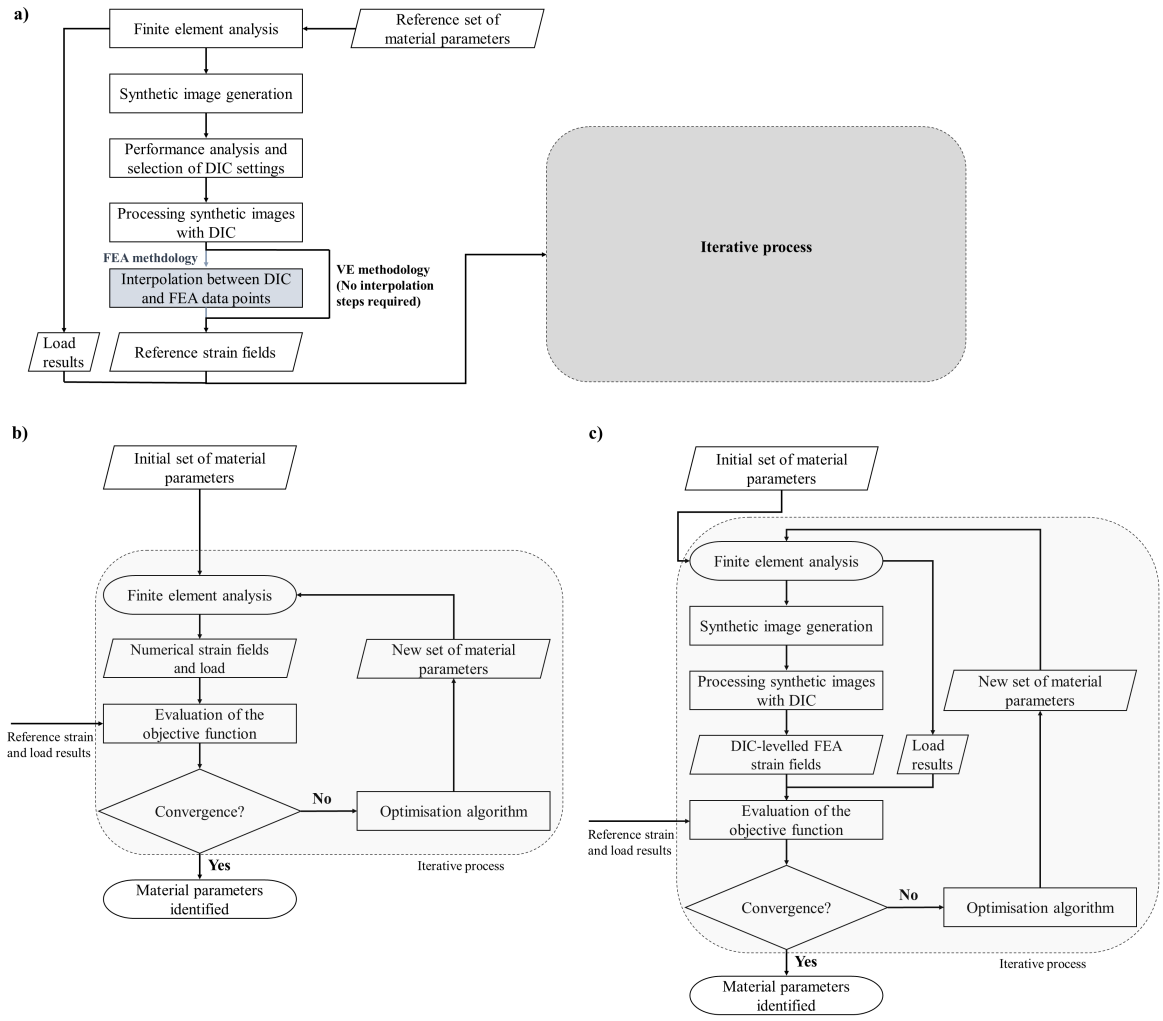

Fig. 3: Flowchart describing the parameter identification process using FEMU for the FEA and VE methodologies: (a) generation of the reference virtual experimental strain fields and load data, (b) the iterative process of the FEA methodology and (c) the iterative process with the VE methodology.

ative error, and the computational time required. The Latin hypercube sampling (LHS) method was used to generate the initial set of parameters for both runs.

The results show a significant improvement in the accuracy of the parameters identified when using the VE methodology, with a maximum relative error of 0.16% for the most accurate identification run (run 2), whereas the maximum relative error for the FEA methodology is 28.48% for the same initial set of parameters. However, the increase in the identification accuracy comes at the expense of the increased computational time required for the VE methodology. The results also show a notable influence of the initial set of parameters on the identification results, possibly due to a local minimum finding. Nevertheless, the results show that in the worst identification run (run 1), the VE methodology proved to be more accurate in the identification of the constitutive parameters, except for the ε_0. Moreover, except for the first identification run with the FEA methodology, the ε_0 is the parameter with the largest relative error. Furthermore, for the run 2 of the FEA methodology, the cost function value for the identified parameters was lower than the cost function calculated with the reference parameters. This result is the consequence of comparing data with different filtering, spatial resolution, and formulation, as well as the inherent interpolation errors, and therefore highlighting the importance of a fair comparison in the FEMU approach. Figure 4 shows the convergence study of the identified parameters, cost function value, strain and force terms values throughout the identification process for the best identification run of each methodology. The value of the strain term is defined as the normalized sum of all strain components, whereas the value of the force term is defined as the normalized

Table 2: Reference set of parameters, lower and upper bounds, initial set of parameters, computational time, cost function value and identification results, including the cost relative error.

	K [MPa]	ε_0	n	Cost function
Lower bound	500.00	0.000001	0.000001	-
Upper bound	1500.00	0.010000	0.400000	-
FEA methodology				
Reference parameters	979.46	0.005350	0.194000	1.640×10^{-4}
Run 1 - CPU time: 34 minutes (1.00 rel. time)				
Initial parameters	1151.17	0.003600	0.000024	2.811×10^{-1}
Identified parameters	867.75	0.010000	0.000001	1.883×10^{-1}
Relative error [%]	11.41	86.92	99.99	-
Run 2 - CPU time: 36 minutes (1.06 rel. time)				
Initial parameters	708.51	0.005730	0.218000	8.853×10^{-2}
Identified parameters	968.83	0.003800	0.187000	1.567×10^{-4}
Relative error [%]	1.09	28.48	3.81	-
VE methodology				
Reference parameters	979.46	0.005350	0.194000	1.055×10^{-9}
Run 1 - CPU time: 198 minutes (5.82 rel. time)				
Initial parameters	1151.17	0.003600	0.000024	3.093×10^{-1}
Identified parameters	993.86	0.010000	0.207577	2.848×10^{-5}
Relative error [%]	1.47	86.92	7.00	-
Run 2 CPU time: 287 minutes (8.44 rel. time)				
Initial parameters	708.51	0.005730	0.218000	8.830×10^{-2}
Identified parameters	979.15	0.005340	0.194000	1.680×10^{-8}
Relative error [%]	0.03	0.16	0.06	-

sum of the load results.

The convergence study shows that the cost function value for the VE methodology is significantly lower than for the FEA methodology. This difference is mainly due to the accurate strain term minimisation, as both data sets used in the comparison are processed by DIC, ensuring that discrepancies between FEA and DIC data are addressed. It can also be seen that the major differences rely on the strain fields comparison's evolution, as expected due to the methodology here introduced.

Figure 5 compares the Swift hardening law plots for the reference and identified parameters of the best identification run for each methodology (run 2 for both methodologies). When compared to the reference parameters, the identified parameters are accurate. Even the values for yield stress are slightly different ($\sigma_0^{\text{FEA}} = 341.71$ MPa vs $\sigma_0^{\text{ref}} = \sigma_0^{\text{VE}} = 355.00$ MPa), these differences are imperceptible in the hardening curve. Nonetheless, the VE methodology proved to be more accurate in the identification process, which might become even clearer when using more complex constitutive models.

Conclusions

This study investigated an inverse identification technique based on FEMU by reconstructing both numerical and experimental strain fields with the same DIC filtering, as well as comparing it to the traditional FEMU approach that compares directly DIC and FEA results. Both approaches were used

in the identification of Swift hardening law parameters of DP600 steel, using a virtual uniaxial tensile test on a heterogeneous dogbone specimen. Although the strain hardening parameters can be identified using a standard tensile test, this study focused on the effect of using the VE methodology. The results show a significant improvement in the identification accuracy when using the DIC-levelled FEA data

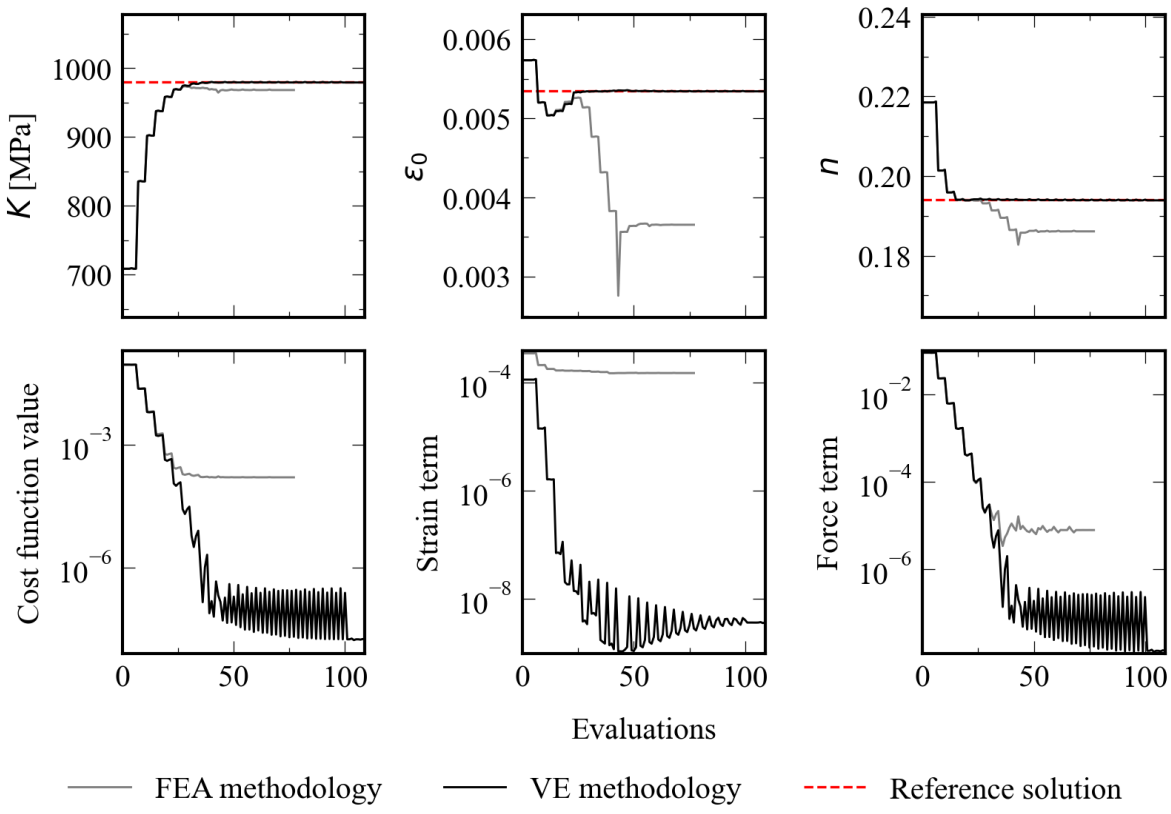

Fig. 4: Evolution of the identified parameters, cost function value, strain and force terms values throughout the identification process, for the best identification run of each methodology.

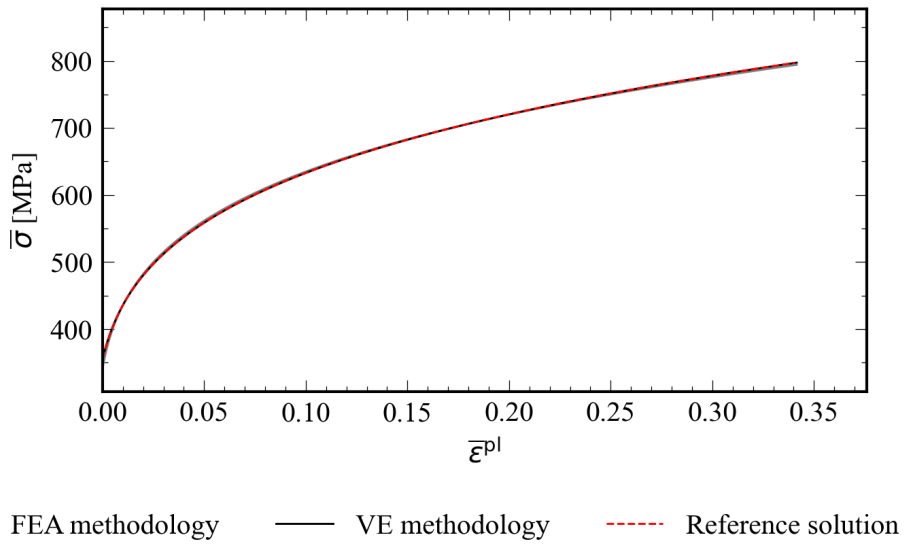

Fig. 5: Comparison between the Swift hardening law using the reference and identified parameters for the best identification run of each methodology.

in the identification procedure mainly due to the accurate minimisation of the differences between the strain results. However, this improved accuracy comes at the expense of increased computational time. The results also show a strong influence of the initial set of parameters on the calibrated parameters.

In future work, the VE methodology can be used to identify the constitutive parameters of more complex constitutive models using other heterogeneous test configurations, allowing all material parameters to be identified using a single test configuration. Moreover, the VE methodology can be further compared to recent studies that use an alternative approach [26]. In this approach, the FEA displacements are interpolated to the DIC data points, then the strain window method is used to derive the strains. This method is consistent concerning the strain computation, yet does not account for the correlation algorithm.

Acknowledgments

This project has received funding from the Research Fund for Coal and Steel under grant agreement No 888153. The authors also gratefully acknowledge the financial support of the Portuguese Foundation for Science and Technology (FCT) under the projects CENTRO-01-0145-FEDER-029713, POCI-01-0145-FEDER-031243 and POCI-01-0145-FEDER-030592 by UE/FEDER through the programs CENTRO 2020 and COMPETE 2020, and UIDB/00481/2020 and UIDP/00481/2020-FCT under CENTRO-01-0145-FEDER-022083. Authors also acknowledge Fundação para a Ciência e a Tecnologia (FCT - MCTES) for its financial support via the projects UIDB/00667/2020 (UNIDEMI). J. Henriques is also grateful to the FCT for the PhD grant 2021.05692.BD.

References

[1] S. Thuillier and P. Y. Manach. Comparison of the work-hardening of metallic sheets using tensile and shear strain paths. *International Journal of Plasticity*, 25:733–751, 05 2009.

[2] S. Thuillier, P. Y. Manach, and L. Menezes. Occurence of strain path changes in a two-stage deep drawing process. *Journal of Materials Processing Technology*, 210:226–232, 01 2010.

[3] H. Vegter, C. Horn, and M. Abspoel. The vegter lite material model: simplifying advanced material modelling. *International Journal of Material Forming*, 4:85–92, 2009.

[4] S. Gothivarekar, S. Coppieters, R. Talemi, and D. Debruyne. Effect of bending process on the fatigue behaviour of high strength steel. *Journal of Constructional Steel Research*, 182:106662, 2021.

[5] A. Andrade-Campos, S. Thuillier, P. Pilvin, and F. Teixeira-Dias. On the determination of material parameters for internal variable thermoelastic–viscoplastic constitutive models. *International Journal of Plasticity*, 23(8):1349–1379, 2007.

[6] S. Zang, S. Thuillier, A. Port, and P. Y. Manach. Prediction of anisotropy and hardening for metallic sheets in tension, simple shear and biaxial tension. *International Journal of Mechanical Sciences*, 53:338–347, 05 2011.

[7] N. Souto, A. Andrade-Campos, and S. Thuillier. Mechanical design of a heterogeneous test for material parameters identification. *International Journal of Material Forming*, 10:353–367, 2017.

[8] H. Schreier, J.-J. Orteu, and M.A. Sutton. *Image correlation for shape, motion and deformation measurements: Basic concepts, theory and applications*. Springer, 2009.

[9] J. Xavier, M. Oliveira, P. Monteiro, J. Morais, and M. De Moura. Direct evaluation of cohesive law in mode i of pinus pinaster by digital image correlation. *Experimental Mechanics*, 54:1–12, 06 2014.

[10] A. Lattanzi, F. Barlat, F. Pierron, A. Marek, and M. Rossi. Inverse identification strategies for the characterization of transformation-based anisotropic plasticity models with the non-linear vfm. *International Journal of Mechanical Sciences*, 173:105422, 2020.

[11] S. Avril, M. Bonnet, A. Bretelle, M. Grédiac, F. Hild, P. Ienny, F. Latourte, D. Lemosse, S. Pagano, E. Pagnacco, and F. Pierron. Overview of identification methods of mechanical parameters based on full-field measurements. *Experimental Mechanics*, 48:381–402, 2008.

[12] A. Güner, C. Soyarslan, A. Brosius, and A.E. Tekkaya. Characterization of anisotropy of sheet metals employing inhomogeneous strain fields for yld2000-2d yield function. *International Journal of Solids and Structures*, 49(25):3517–3527, 2012.

[13] K. Denys, S. Coppieters, M. Seefeldt, and D. Debruyne. Multi-dic setup for the identification of a 3d anisotropic yield surface of thick high strength steel using a double perforated specimen. *Mechanics of Materials*, 100:96–108, 2016.

[14] J. M. P. Martins, A. Andrade-Campos, and S. Thuillier. Comparison of inverse identification strategies for constitutive mechanical models using full-field measurements. *International Journal of Mechanical Sciences*, 145:330–345, 2018.

[15] F. Pierron and M. Grediac. *The virtual fields method: Extracting constitutive mechanical parameters from full-field deformation measurements*. Springer, 2012.

[16] R. Balcaen, L. Wittevrongel, P. L. Reu, P. Lava, and D. Debruyne. Stereo-dic calibration and speckle image generator based on fe formulations. *Experimental Mechanics*, 57:703–718, 2017.

[17] P. Lava, E. Jones, L. Wittevrongel, and F. Pierron. Validation of finite-element models using full-field experimental data: Levelling finite-element analysis data through a digital image correlation engine. *Strain*, 56(4):e12350, 2020.

[18] J. Henriques, J. Xavier, and A. Andrade-Campos. Identification of orthotropic elastic properties of wood by a synthetic image approach based on digital image correlation. *Materials*, 15(2), 2022.

[19] J. M. P. Martins, S. Thuillier, and A. Andrade-Campos. Identification of material parameters for plasticity models: A comparative study on the finite element model updating and the virtual fields method. *AIP Conference Proceedings*, 1960(1):110007, 2018.

[20] Dassault Systèmes. Abaqus 2019 documentation, 2019.

[21] H. Takizawa, T. Kuwabara, K. Oide, and J. Yoshida. Development of the subroutine library 'UMMDp' for anisotropic yield functions commonly applicable to commercial FEM codes. *Journal of Physics: Conference Series*, 734:032028, aug 2016.

[22] F. Ozturk, S. Toros, and S. Kilic. Effects of anisotropic yield functions on prediction of forming limit diagrams of dp600 advanced high strength steel. *Procedia Engineering*, 81:760–765, 2014.

[23] M. G. Oliveira, S. Thuillier, and A. Andrade-Campos. Analysis of heterogeneous tests for sheet metal mechanical behavior. *Procedia Manufacturing*, 47:831–838, 2020.

[24] MatchID: Metrology beyond colors. Matchid version 2021.2, 2021, NV, Ghent, Belgium.

[25] E. Jones, T. Oliphant, P. Peterson, et al. SciPy: Open source scientific tools for Python, 2001.

[26] Y. Zhang, S. Gothivarekar, M. Conde, A. Van de Velde, B. Paermentier, A. Andrade-Campos, and S. Coppieters. Enhancing the information-richness of sheet metal specimens for inverse identification of plastic anisotropy through strain fields. *International Journal of Mechanical Sciences*, 214:106891, 2022.